Enhancing Solubility, Antioxidant Activity and Antimicrobial Activity of Curcumin through Cocrystals

Yanyan Huang[a] https://orcid.org/0009-0003-0282-5188, Rui Yu[a], Siying Xia[b], Wenxin Yao[b,*], Min Xing[b], Yonggang Bian[a], Zhiwei Huang[a,*] https://orcid.org/0000-0002-7140-5115

[a]College of Biological Science and Medical Engineering, Donghua University, 2999 Renmin Road, Shanghai 201620, China
[b]Laboratory of Dental Biomaterials and Tissue Regeneration, Shanghai Xuhui District Stomatological Hospital, Shanghai, 200032, China

Submitted 2025/11/21
Revised 2026/2/25
Accepted 2026/4/26

*Corresponding author:
Zhiwei Huang Ph.D.
College of Biological Science and Medical Engineering
Donghua University 2999 Renmin Road, Shanghai 201620, China
Telephone: (086) 21-67792911
Fax: (086)21-64233245
E-mail: zhiweih@dhu.edu.cn
Wenxin Yao
Shanghai Xuhui District Stomatological Hospital,
Shanghai, 200032, China
E-mail: ywx520np@163.com

Acknowledgments

We are grateful to the Medicine-Engineering Interdisciplinary Project of Shanghai Xuhui District Stomatological Hospital and the National Natural Science Foundation of China.

Author Contributions

Y.H.: Material preparation, investigation, formal analysis, data curation, writing and editing. R.Y. and Y.B.: Material preparation, data collection, and analysis. S.X., W.Y. and M.X.: Funding and resources. Z.H.: Funding, supervision, conceptualization,

resources, writing and editing. All authors read and approved the final manuscript.

Conflicts of Interest

The authors declared that they have no known competing financial interests or personal relationships that could have appeared to influence the work reported in this paper.

FUNDING

This work was sponsored by grants from the Medicine-Engineering Interdisciplinary Project of Shanghai Xuhui District Stomatological Hospital（Grant ID: SHXHKYYG202507), and the National Natural Science Foundation of China (Grant ID: 32171958).

Abstract

Background: Curcumin (CUR) is a natural polyphenolic compound exhibiting diverse pharmacological activities. However, its extremely low aqueous solubility and poor chemical stability severely limit its bioavailability and clinical application.

Methods: Two novel cocrystals of CUR, CUR-m-hydroxybenzoic acid (CUR-MHBA) and CUR-gallic acid (CUR-GA), were prepared via slurry crystallization and characterized by Powder X-ray diffraction (PXRD), Differential scanning calorimetry (DSC), Thermogravimetric analysis (TG), Fourier transform infrared spectroscopy (FT-IR), and ^{1}H Nuclear Magnetic Resonance (^{1}H-NMR). Their solubility, dissolution behavior, antioxidant capacity, and antibacterial activity were systematically evaluated.

Results: Saturation solubility analysis showed that CUR-MHBA and CUR-GA had higher equilibrium solubility than CUR alone, both in water and ethanol at 25°C and 37°C. Dissolution testing showed that both cocrystals exhibited similar “spring-parachute” characteristics to CUR in four different solutions (pH 1.2, 4.5, 6.8, and 7.4), with higher steady state concentrations than CUR. Moreover, CUR-MHBA and CUR-GA demonstrated enhanced antioxidant activity. Relative to CUR, their free radical scavenging capacities increased by 1.29 and 1.43-fold, 1.47 and 3.89-fold, and 1.45 and 1.47-fold using DPPH (2,2-diphenyl-1-picrylhydrazyl), ABTS (2,2′-azino-bis(3-ethylbenzothiazoline-6-sulfonic acid)), and FRAP (Ferric Reducing Antioxidant Power) assays, respectively. Antibacterial assays against *Staphylococcus aureus* and *Escherichia coli* also revealed significantly lower minimum inhibitory concentrations (MIC) for both cocrystals compared to CUR alone.

Conclusion: CUR-MHBA and CUR-GA significantly improved the solubility, dissolution, and biological activities of CUR. These results suggest that cocrystallization with bioactive polyphenolic acids is an effective approach to enhance

the physicochemical properties and therapeutic potential of CUR.

Key words: Curcumin, Cocrystal, m-hydroxybenzoic acid, gallic acid, Solubility, Antioxidant activity, Antimicrobial activity

1. Introduction

Curcumin (CUR), a natural polyphenol derived from *Curcuma longa*, possesses a chemical structure containing a β-diketone group, an alkene bond, and phenolic rings[1,2] (Figure 1a). It has been used for centuries both as a food spice and in traditional medicine.[3] Recent studies have shown that CUR exhibits various pharmacological effects such as antibacterial, antioxidant, anti-inflammatory, anticancer, and wound-healing activities,[4-8] making it a promising candidate for treating cancer, Alzheimer's disease, and other related diseases.[9,10]However, the extremely low aqueous solubility and poor oral bioavailability (<1%) hinder the clinical application of CUR, which is due to its low solubility (<8 μg/mL in water), limited permeability, and rapid metabolism (half-life < 2 h).[2] In a human trial, the maximal plasma concentration was only 92 ± 29 ng/mL even at high oral doses (1-4 g/day).[11] Its further limitations include chemical instability and fast systemic clearance.[12]

Cocrystal engineering, based on supramolecular synthon principles,[13] provides an efficient strategy to tailor material properties.[14,15] Pharmaceutical cocrystals consist of an API and a pharmaceutically acceptable coformer in a fixed stoichiometric ratio,[16-18] stabilized by non-covalent interactions such as hydrogen bonds, π–π stacking, and van der Waals forces.[19-22] Hydrogen bonding is particularly important due to its strength and directionality.[23,24] Supramolecular synthons,[25] either homosynthons or heterosynthons, [26,27] guide the assembly, with common motifs including acid-acid, acid-amide, and acid-pyridine dimers.[28-30] Cocrystallization can modify key properties including solubility, dissolution rate, and bioavailability without altering the API's covalent structure or intrinsic activity.[31-36] For instance, a cocrystal of amantadine HCl and sulfathiazole exhibited a significant reduction in the MIC against *Bacillus subtilis*, decreasing from 0.40 mg/mL for the individual API to 0.05 mg/mL.[37]

To improve the solubility of CUR via cocrystals, approximately 20 systems have been developed using coformers such as nicotinamide, bipyridine, and glucose.[38-43] These studies demonstrate that cocrystallization can significantly influence the dissolution behavior and physicochemical performance of CUR. More recent reports have further expanded the range of CUR cocrystals structurally diverse coformers, primarily aiming to enhance solubility, dissolution rate, and, in some cases, bioavailability.[39,43,44] In particular, early studies demonstrated that CUR cocrystals prepared by liquid-assisted grinding with simple phenolic coformers, including resorcinol and pyrogallol, primarily showed improved dissolution in hydroalcoholic media.[38] Although most systems demonstrated increased solubility and dissolution, certain cocrystals, such as CUR-phloroglucinol,[45] performed poorly due to surface precipitation or dissociation-

triggered crystallization ("spring" effect).[46] Despite these advances, previous studies have mainly focused on improving the physicochemical properties of CUR via cocrystals, with relatively limited investigation under biorelevant conditions and insufficient attention to their potential impact on biological activity.

In this study, two antioxidant and antibacterial polyphenolic acids, m-hydroxybenzoic acid (MHBA) and gallic acid (GA) (Figure 1b-c), were selected as coformers for CUR based on crystal engineering principles. Both compounds possess hydroxyl and carboxyl groups, which facilitate stronger and more diverse hydrogen-bonding interactions, resulting in distinct solid-state characteristics and dissolution profiles. CUR-MHBA and CUR-GA cocrystals were synthesized, and their structural properties were characterized. Their equilibrium solubility, dissolution, and in vitro antioxidant and antibacterial activities were evaluated. In contrast to previous reports,[39,43,44] this work evaluated dissolution of these cocrystals under biorelevant aqueous conditions (pH 1.2, 4.5, 6.8, and 7.4) and demonstrated sustained supersaturation. Furthermore, the study examined the functional contributions of coformers with intrinsic antioxidant and antimicrobial activities, offering additional insight into the potential interplay between cocrystal design and biological performance. These findings underscore a distinct design rationale and broader pharmaceutical relevance for the cocrystals developed. It is expected to provide foundational data for future pharmacological research.

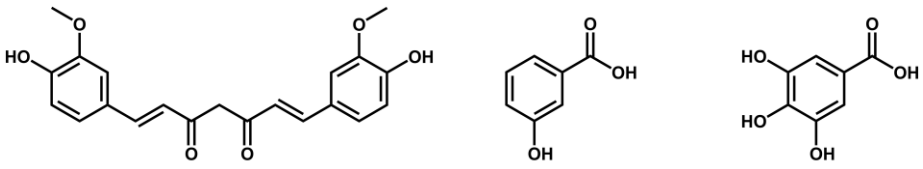

Figure 1. Chemical structures of (a) CUR, (b) MHBA and (c) GA.

2. Methods

2.1. Materials

Curcumin (CUR, analytical grade) was purchased from Sinopharm Chemical Reagent Co., Ltd.(China). m-hydroxybenzoic acid (MHBA, 98% purity), and gallic acid (GA, >98% purity) were obtained from Shanghai Adamas Reagent Co., Ltd. (Shanghai, China). All other chemicals and reagents were of analytical grade and used without further purification.

2.2. Preparation of cocrystals

The cocrystals of CUR-MHBA and CUR-GA were synthesized via the slurry crystallization method. CUR (368 mg, 1 mmol) and MHBA (138 mg, 1 mmol) were combined in a 20 mL glass vial with 10 mL of ethyl acetate as the solvent. For CUR-GA, CUR (410 mg, 1.11 mmol) and GA (190 mg, 1.11 mmol) were mixed with 15 mL of ethyl acetate/ethanol/water (3:2:1, v/v/v). Both suspensions were continuously stirred at 400 rpm for 48 hours at room temperature in foil-wrapped vials with punctures for ventilation. The resulting crystalline solids were isolated by vacuum filtration and subsequently dried under vacuum at 35°C for 48 hours. The final products were hermetically packaged and stored at ambient temperature for subsequent analysis.

2.3. Crystal Engineering Analysis

ΔpKa values were calculated using reported pKa data obtained from DrugBank (CUR) and PubChem (MHBA and GA). ΔpKa was defined as pKa(base) – pKa(acid) and used to assess the likelihood of salt versus cocrystal formation. Molecular electrostatic potential surface (MEPS) calculations were performed at the DFT level (B3LYP/6-31G(d)) after geometry optimization in the gas phase. The electrostatic potential extrema (Vmax and Vmin) were analyzed to identify potential hydrogen-bond donor and acceptor sites.

2.4. Characterization of raw materials and cocrystals

2.4.1. Powder X-ray diffraction (PXRD)

PXRD was performed on a Bruker D8 Advance diffractometer (Bruker AXS, Germany). Samples were uniformly packed into a custom-made aluminum holder with a depth of 2 mm. The analysis was conducted using Cu - Kα radiation source (λ = 1.54060 Å) at 40kV and 20 mA. Diffractograms were collected in reflection mode over a 2θ range of 5 to 60° with a step size of 0.02°. The diffracto-grams were analyzed using the X'pert High Score program, and the PXRD patterns were plotted using the Origin 2021 software.

2.4.2. Differential scanning calorimetry (DSC)

Thermal analysis was performed using a Mettler Toledo TG/DSC Stare System (Switzerland). Samples (5-10 mg) were weighted in a hermetically sealed aluminum crucible and subjected to a temperature heating from 25°C to 250°C at a heating rate of 10°C /min under argon atmosphere (50 mL/min). An empty pan served as reference.

The data were analyzed by Mettler Toledo Stare System's software and plotted with Origin 2021 software.

2.4.3. Thermogravimetric (TG)

TG measurements were performed in a Mettler Toledo TG/DSC Stare System (Switzerland). The samples (5-10 mg) were weighted in alumina crucibles and heated from 25°C to 600°C at 10°C/min under argon atmosphere (50 mL/min) to determine mass loss profiles. The data were analyzed by Mettler Toledo Stare System's software and plotted with Origin 2021 software.

2.4.4. Fourier-transform infrared spectroscopy (FT-IR)

FT-IR spectra were acquired on a Thermo Scientific IS50 spectrometer (USA) using KBr pellets. Scans covered 4000-500 cm^{-1} range at 1 cm^{-1} resolution. The data were analyzed by Spectrum software and plotted with Origin 2021 software.

2.4.5. ^{1}H Nuclear Magnetic Resonance (^{1}H-NMR)

^{1}H-NMR spectra were obtained using a Bruker AVANCE III HD 600 MHz spectrometer (Switzerland). In order to collect data for the ^{1}H-NMR investigations,dissolve 5mg of samples in DMSO-d6 or D_2O and transfer to a clean NMR tube.The data were analyzed by MestReNova v14.2.1-27684 and plotted with Origin 2021 software.

2.5. Determination of Saturation Solubility and Dissolution Profile

The saturation solubility of CUR and its cocrystals was determined in water or ethanol using the shake-flask method.[47,48] Excess powdered samples were added to 5 mL of deionized water or ethanol in 15-mL centrifuge tubes. The sealed tubes were agitated at 180 rpm on a shaker at 37°C for 24 hours. Subsequently, supernatants were filtered through 0.45 μm membrane filters and analyzed at 426 nm using UV spectrophotometry. Saturation solubility values were calculated against standard calibration curves established in the respective solvents. Each experiment was carried out in three duplicates. The data were processed and analyzed by GraphPad Prism 10.3.1 software.

Powder dissolution profiles were determined using a protocol adapted from Zhou Y et al..[49]Dissolution profiles were determined in pH 1.2, 4.5, 6.8, and 7.4 buffer solutions following the shake-flask method. Excess powder samples were introduced

into 10 mL of buffer solution in 15-mL centrifuge tubes. After sealing, samples were agitated at 180 rpm at 37°C. Aliquots (0.5 mL) were withdrawn at 5, 10, 15, 20, 30, 45, 60, 90, and 120 min following immersion. Samples were centrifuged at 10,000 rpm for 10 min, and supernatants were diluted before concentration measurement using predetermined standard curves. Each experiment was carried out in three duplicates. The data were processed and analyzed by GraphPad Prism 10.3.1 software.

2.6. Determination of In Vitro Antioxidant Activity

Antioxidant activity of CUR and its cocrystals was determined using three methods: DPPH, ABTS, and the FRAP assays. Every sample was measured in three duplicates. The data were processed and analyzed by GraphPad Prism 10.3.1 software.

The DPPH assay was adapted to the protocol of Mitic et al..[50] A stock solution of DPPH (0.04 mg/mL in ethanol) was diluted to an absorbance of 0.6-1.0 at 517 nm. In 96-well plates, 100 μL of sample solutions at varying concentrations were mixed with 100 μL DPPH solution. After 30 min of light-protected incubation, absorbance was measured at 517 nm using a SpectraMax M2 multi-mode microplate reader. The following equation was used to represent the results as the DPPH free radical scavenging rate(E%):

$$E(\%) = [1\text{-}(A_i - A_j)/\, A_k] \times 100\%$$

where A_i indicates the absorbance of a sample and DPPH alcoholic solution mixture;A_j indicates the absorbance of a sample and ethanol mixture;A_k indicates the absorbance of an ethanol and DPPH alcoholic solution mixture.

The ABTS assay followed Rozi et al..[51] ABTS working solution was prepared by mixing 0.2 mL of 7.4 mmol/L ABTS with 0.2 mL of 2.6 mmol/L potassium persulfate, followed by 12-hour dark incubation. The solution was then diluted 50-fold with PBS buffer. In 96-well plates, 100 μL sample solutions were reacted with 100 μL diluted ABTS solution for 10 min under dark conditions. Absorbance was recorded at 734 nm using the SpectraMax M2 reader. The following equation was used to represent the results as the ABTS free radical scavenging rate(E%):

$$E(\%) = [1\text{-}(A_i - A_j)/\, A_k] \times 100\%$$

where A_i indicates the absorbance of a sample and ABTS working solution mixture;A_j indicates the absorbance of a sample and ethanol mixture;A_k indicates the absorbance of an ethanol and ABTS working solution mixture.

The FRAP assay was adapted from Ben-zie et al..[52] Working solution contained

2.5 mL 10 mmol/L TPTZ, 2.5 mL 20 mmol/L $FeCl_3 \cdot 6H_2O$, and 25 mL 0.3 mol/L acetate buffer (pH 3.6). In 96-well plates, 100 μL sample solutions were mixed with 100 μL FRAP reagent and incubated at 37°C for 30 min. Absorbance was measured at 593 nm. The FRAP value for each sample was determined against a standard $FeSO_4$ value, which calculated from a calibration curve with values ranging from 1.25 to 40 μg/mL.

$$A = 0.05C + 0.0779, r = 0.996$$

where A indicates absorbance value;C indicates $FeSO_4$ concentration (μg/mL).

2.7. Determination of Antimicrobial activity

The minimum inhibitory concentration (MIC) was determined against *Staphylococcus aureus* (*S.aureus*) and *Escherichia coli* (*E.coli*) using the microbroth dilution method according to Veiga et al..[53] Serial two-fold dilutions of CUR and its cocrystals (1 mg/mL to 0.000488 μg/mL) were prepared in Luria-Bertani (LB) broth. Bacterial cultures were grown in LB broth at 37°C with shaking to mid-log phase ($OD_{600} \approx 0.6$) and diluted to 10^6 CFU/mL. CUR, four cocrystal solutions, and diluted bacterial suspensions were added to U-bottomed 96-well microplates, with microorganism-containing and sterile broths serving as positive and negative controls respectively. After 24-hour incubation at 37°C, OD_{600} measurements were taken every 2 hours (within 12 hours) and at 24 or 36 hours. Growth kinetics analysis provided insights into antimicrobial mechanisms.[54] Subsequently, 20 μL of 0.125% 2,3,5-triphenyltetrazolium chloride (TTC) solution was added to each well, followed by 30-minute re-incubation at 37°C, with the MIC defined as the lowest concentration showing no red coloration. The data were processed and analyzed by GraphPad Prism 10.3.1 software.

For the zone of inhibition assay adapted from Serrano et al.,[55] the agar well diffusion method was employed. Overnight bacterial cultures were mixed with molten LB agar (50°C) at 10^6 CFU/mL concentration, poured into plates containing four pre-positioned Oxford cups (~20 mL/plate). After solidification, cups were removed to create wells. Test solutions (100 μL) at varying concentrations were added to wells using DMSO controls. Following 24-hour incubation at 37°C, inhibition zone diameters (mm) were measured. The data were processed and analyzed by GraphPad Prism 10.3.1 software.

2.8. Stability study

The physical stability of the prepared cocrystals was evaluated under controlled

humidity conditions. A relative humidity of approximately 75% was established using a saturated NaCl solution in a sealed container at room temperature. The cocrystal samples were placed on a sample holder above the salt solution to avoid direct contact with the liquid phase. The container was tightly sealed and stored at room temperature. Samples were collected at 0, 7, and 14 days and analyzed by PXRD to monitor potential phase transformation or structural changes.

2.9. Sataistical analysis

All experiments were performed in at least three independent replicates (n = 3). Data are presented as the mean ± standard deviation (SD). Statistical significance of differences between the individual CUR and cocrystal groups in terms of solubility, antioxidant activity, and antibacterial activity was determined by one-way analysis of variance (ANOVA) followed by Tukey's honest significant difference (HSD) post hoc test for multiple comparisons. A p-value of less than 0.05 ($p < 0.05$) was considered statistically significant.

3. Results and discussion

3.1. Crystal Engineering analysis

To rationalize the selection of MHBA and GA as coformers, ΔpKa analysis was performed to evaluate the likelihood of salt versus cocrystal formation. The calculated ΔpKa values were strongly negative, indicating that proton transfer from the carboxylic acid coformers to CUR is thermodynamically unfavorable, supporting neutral cocrystal formation rather than salt formation (Table 1). Molecular electrostatic potential surface (MEPS) analysis further revealed clear electrostatic complementarity between CUR and the selected coformers (Figure 2). The β-diketone carbonyl groups of CUR exhibited pronounced negative electrostatic potential, consistent with hydrogen-bond acceptor capability, whereas the carboxylic acid protons of MHBA and GA displayed strong positive potential, indicating hydrogen-bond donor sites. This complementarity suggests that acid–carbonyl O–H···O heterosynthons are the dominant supramolecular interaction. Additional estimates of interaction energy are summarized in Table 2. Both CUR-MHBA and CUR-GA systems exhibited negative ΔE values, indicating a preference for heteromolecular association over homomolecular aggregation. The more negative ΔE observed for CUR-GA suggests a relatively stronger predicted heteromolecular interaction tendency.

Table 1. pKa values and calculated ΔpKa used to assess salt versus cocrystal formation.

Component	Relevant pKa(type)	pKa	ΔpKa	Source
CUR	pKa (strongest basic, predicted)	-4.40	—	DrugBank
MHBA	pKa_1 (carboxylic acid)	4.08	-8.48	PubChem
GA	pKa_1 (carboxylic acid)	4.21	-8.61	PubChem

*ΔpKa = pKa(base) – pKa(acid). Strongly negative ΔpKa values suggest that proton transfer is thermodynamically unfavorable, supporting neutral hydrogen-bond-driven cocrystal formation rather than salt formation.

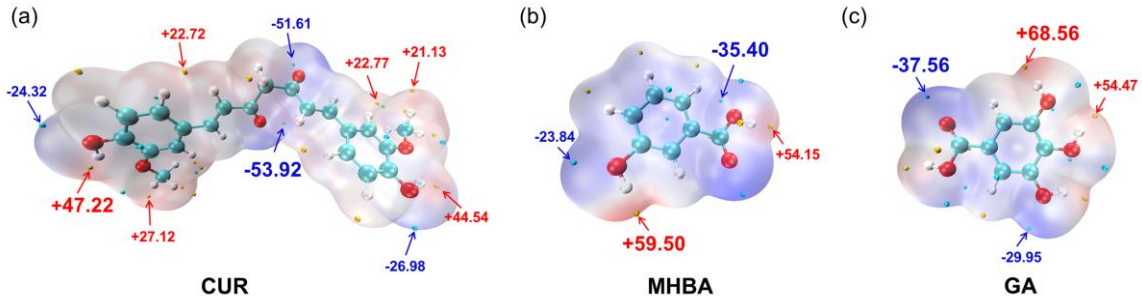

Figure 2. Molecular electrostatic potential surfaces (MEPS) of (a) CUR, (b) MHBA and (c) GA.

Red and blue regions represent positive and negative electrostatic potentials, corresponding to hydrogen-bond donor and acceptor sites, respectively. MEP extrema (Vmax, Vmin) are labeled in kcal/mol.

Table 2. SSIP/MEPS-derived interaction energy estimations for CUR and coformers.

	E_{AA} (kJ·mol^{-1})	E_{AB} (kJ·mol^{-1})	ΔE (kJ·mol^{-1})
CUR	-62.53	—	—
MHBA	-15.26	-41.72	-2.83
GA	-26.79	-55.05	-10.39

*E_{AA} and E_{AB} represent estimated homomolecular interaction energies, E_{AB} represents heteromolecular interaction energy, and ΔE denotes the interaction energy difference used to evaluate heteromolecular association tendency. More negative ΔE values indicate stronger predicted API–coformer interactions.

3.2. Powder X-Ray diffraction (PXRD) analysis

Powder X-ray diffraction (PXRD) is an effective method for rapid detection of new crystalline phases in solid states.[56] As seen in Figure 3, the PXRD patterns of CUR-MHBA and CUR-GA cocrystals exhibited distinctly different crystalline peaks compared to both CUR and their respective coformers, indicating formation of novel

crystalline phases. Specifically, the CUR-MHBA pattern displayed new intense diffraction peaks at 9.58°, 29.89°, and 32.11°, while the characteristic MHBA peak at 30.72° disappeared. The CUR-GA pattern showed new peaks at 20.36°, 22.17°, and 28.51°, concurrent with the disappearance of characteristic CUR diffraction at 21.15° and GA peaks at 7.09°, 14.29°, and 25.14°. These collective alterations in diffraction patterns confirmed the establishment of new crystalline phases in the cocrystalline systems.

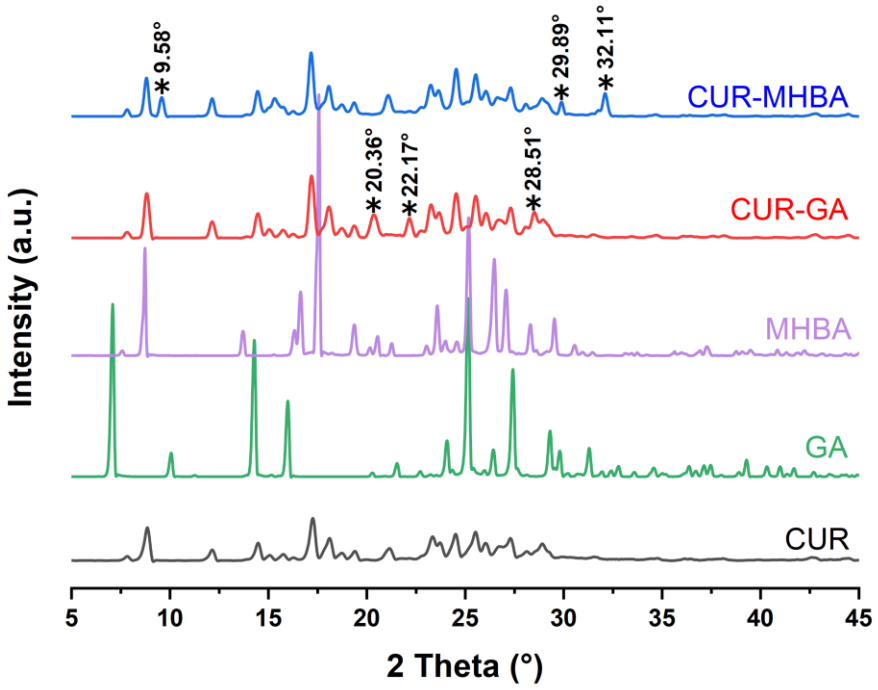

Figure 3. PXRD Patterns of CUR-MHBA, CUR-GA, MHBA, GA and CUR.

3.3. Thermal Analysis (DSC and TG)

Thermal analysis, including DSC and TG, provides critical insight into the thermodynamic stability and phase purity of solid forms.[57] DSC enables comparative evaluation of thermal events between starting materials and resulting cocrystals,[58] while TG monitors mass changes under programmed heating, indicating desolvation and decomposition behaviors.

The DSC curves of CUR-MHBA and CUR-GA cocrystals are presented in Figure 4a. Individual components showed characteristic endotherms: CUR exhibited a single melting peak at 177.13°C, MHBA displayed endothermic at 202.37°C (melting), and GA showed endotherms at 78.62°C (dehydration) and 134.75°C (melting). Neither of

the cocrystals showed endothermic events near the melting points of their individual constituents, confirming high phase purity. Instead, each cocrystal exhibited a single sharp endotherm at a new transition temperature of 158.56°C for CUR-MHBA and 161.26°C for CUR-GA， indicating the formation of distinct crystalline phases with unique thermal profiles.[59]

TG analysis revealed no mass loss prior to melting, confirming the absence of solvent inclusion (Figure 4b) . CUR decomposed in a single step starting at 170.7°C with 65.6% mass loss. In contrast, the cocrystals showed improved thermal stability, with CUR-MHBA and CUR-GA exhibiting singular decomposition events initiating at 206.7°C and 245.9°C, respectively. Each cocrystal displayed a coherent mass loss step distinct from its components, further supporting the formation of new crystalline phases with characteristic decomposition pathways.

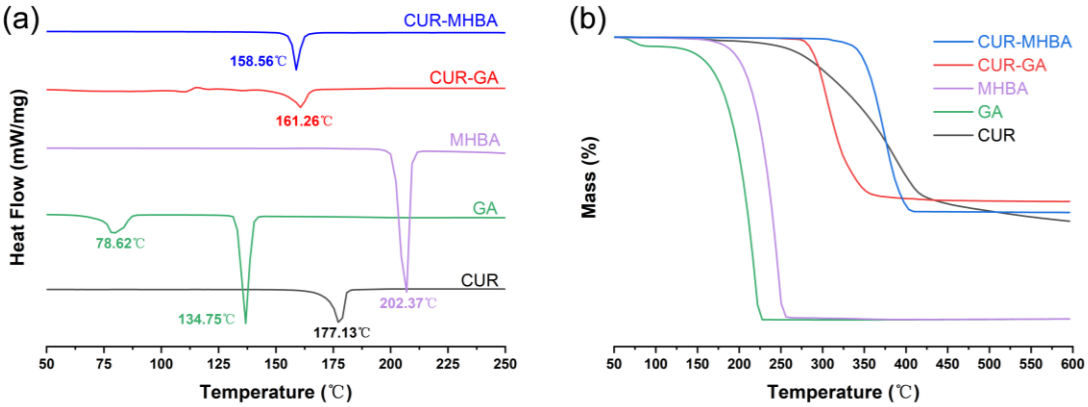

Figure 4. (a) DSC patterns of CUR-MHBA, CUR-GA,MHBA,GA and CUR ; (b) TG patterns of CUR-MHBA, CUR-GA,MHBA,GA and CUR.

3.4. Fourier-transform infrared spectroscopy (FT-IR) analysis

Fourier transform infrared spectroscopy is a valuable complementary technique for identifying novel solid forms. Comparative analysis revealed distinct spectral alterations in the cocrystals rather than simple superposition of component spectra, as illustrated in Figure 5. Characteristic CUR absorptions appeared at 3424 cm^{-1} for O-H stretching, 1628 cm^{-1} for C=O stretching, 1511 cm^{-1} for C=C stretching, and 1279 cm^{-1} for C-O stretching. Hydrogen bonding induced significant spectral shifts in the cocrystals.

The CUR-MHBA cocrystal exhibited a shift in carboxylic acid O–H stretching from 3430 to 3406 cm^{-1} and a transition in C=O stretching from 1699 to 1607 cm^{-1}. For the CUR-GA cocrystal, the O–H stretching of GA shifted from 3419 to 3440 cm^{-1}, while

the C=O stretching of CUR moved from 1628 to 1619 cm^{-1}. These systematic vibrational modifications confirm the presence of noncovalent interactions between CUR and the coformers, providing conclusive evidence for cocrystal formation.

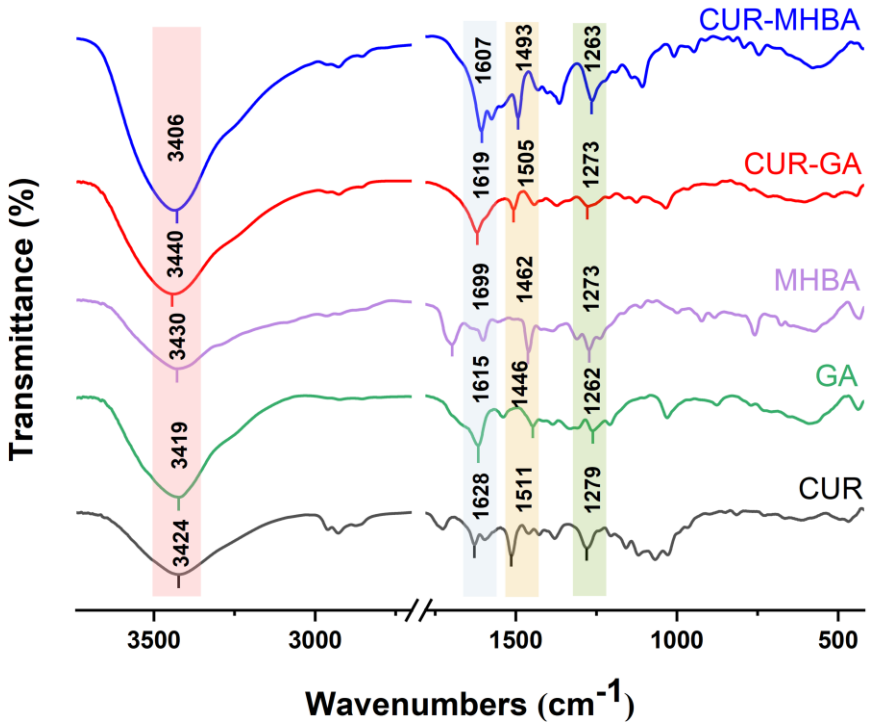

Figure 5. FT-IR patterns of CUR-MHBA, CUR-GA,MHBA,GA and CUR.

3.5. ^{1}H Nuclear Magnetic Resonance(^{1}H-NMR) Analysis

^{1}H-NMR analysis was conducted to confirm the presence and stoichiometric ratios of the cocrystals (Figure 6). Characteristic coformer signals were observed in the spectra: MHBA aromatic protons appeared near 7.39 and 6.98 ppm, and GA aromatic protons near 6.33 ppm. Protons from carboxylic acid and hydroxyl groups were not detected due to exchange broadening. Integration values demonstrated a 1:1 molecular ratio between CUR and each coformer. Notably, CUR-related signals exhibited downfield shifts in the cocrystal spectra, suggesting possible intermolecular interactions that may be associated with hydrogen bonding, consistent with previous reports[49]. However, as the measurements were performed in solution, the solid-state supramolecular organization cannot be directly inferred from ^{1}H-NMR data.

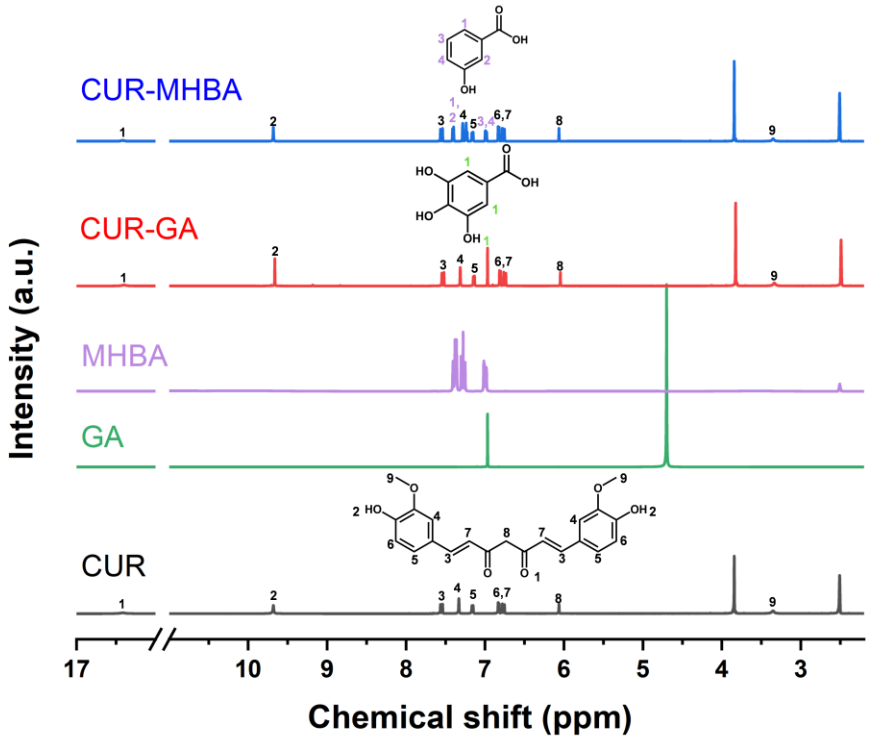

Figure 6. [1]H-NMR patterns of CUR-MHBA, CUR-GA,MHBA,GA and CUR.

3.6. Determination of Saturation Solubility and Dissolution Profile

3.6.1. Saturation Solubility Analysis

Solubility assessments of CUR, CUR-MHBA, and CUR-GA as well as their corresponding physical mixtures (PM) were conducted in two media (Fig. 7). In pure water (Figure 7a), the measured solubility followed the order CUR-GA > CUR-MHBA > CUR. CUR-GA exhibited the highest solubility, measuring 70.51±8.67 μg/mL at 25°C and 120.84±9.76 μg/mL at 37°C, representing 14.9-fold and 31.4-fold increases over CUR, respectively. CUR-MHBA showed the solubility at 7.60±2.94 μg/mL (25°C) and 13.70±2.45 μg/mL (37°C), representing 2.5-fold and 3.6-fold increases over CUR respectively. The PM showed moderate increases in solubility. CUR-MHBA PM exhibited values of 4.18±0.62 μg/mL (25°C) and 4.82±0.30 μg/mL (37°C), while CUR-GA PM reached 8.15±0.83 μg/mL and 10.27±1.23 μg/mL at 25°C and 37°C, respectively. In all cases, the corresponding cocrystals exhibited higher solubility than the physical mixtures under identical conditions. Ethanol solubility profiles differed significantly, as depicted in Figure 7b. The order of solubility was CUR-GA > CUR-MHBA>CUR. In this solvent, CUR-GA demonstrated 3.5-fold and 3.4-fold improvements at 25°C and 37°C, respectively, while CUR-MHBA showed 2.3-fold enhancements at both temperatures. Similarly, the PM exhibited lower solubility than

the corresponding cocrystals in ethanol, with CUR-MHBA PM showing 4.87±0.45 mg/mL and 5.01±0.78 mg/mL, and CUR-GA PM showing 5.61±0.66 mg/mL and 6.07±1.02 mg/mL at 25°C and 37°C, respectively. Overall, the cocrystals exhibit higher measured solubility under the tested experimental conditions compared to CUR and PM.

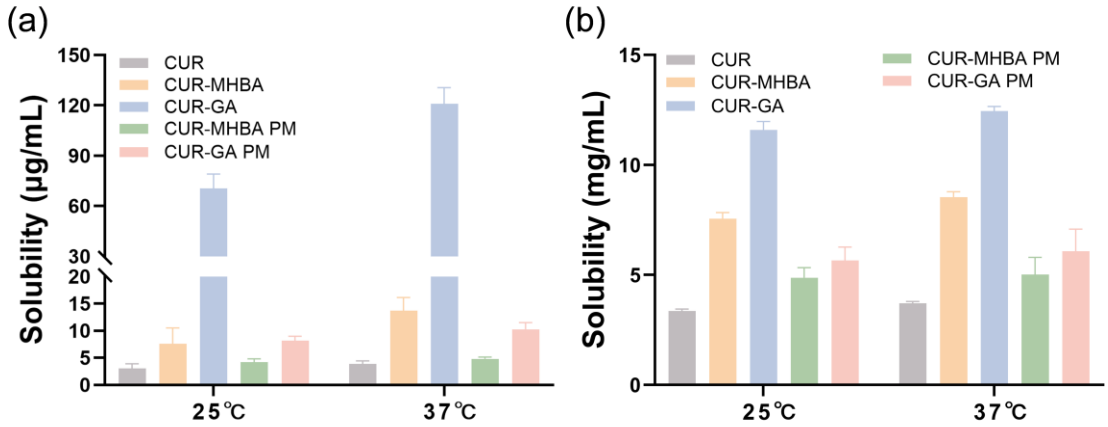

Figure 7. The solubility test results of CUR, cocrystals and corresponding PM in (a) water and (b) ethanol solution.

3.6.2. Dissolution Profile Analysis

Powder dissolution testing characterizes supersaturation behavior in cocrystals exhibiting "spring-parachute" characteristics.[60] Compounds demonstrating this behavior achieve rapid dissolution and sustain elevated concentrations over time, potentially improving solubility, bioavailability, and clinical efficacy.[61-63] The dissolution profiles of CUR, CUR-MHBA, and CUR-GA were evaluated in four buffer systems, as shown in Figure 7.

In pH 1.2 HCl buffer (Figure 7a), dissolution ranked CUR-GA > CUR-MHBA > CUR. CUR-GA showed notably rapid dissolution and maintained high concentrations, consistent with spring-hover behavior.[64] Steady-state concentrations correlated well with solubility data.In pH 4.5 acetate buffer (Figure 7b), both cocrystals outperformed CUR. CUR-MHBA exhibited spring-parachute behavior with an initial rapid release followed by a gradual decline, suggesting crystallization over time.[65] CUR-GA again displayed spring-hover properties with sustained supersaturation.In pH 6.8 phosphate buffer (Figure 7c), the order remained CUR-GA > CUR-MHBA > CUR. CUR-MHBA showed typical spring-parachute release, while CUR-GA maintained spring-hover dissolution, likely due to reversible hydrogen bonding that promotes dynamic equilibrium. In pH 7.4 phosphate buffer (Figure 7d), both cocrystals reached similar

steady-state concentrations, significantly surpassing CUR.

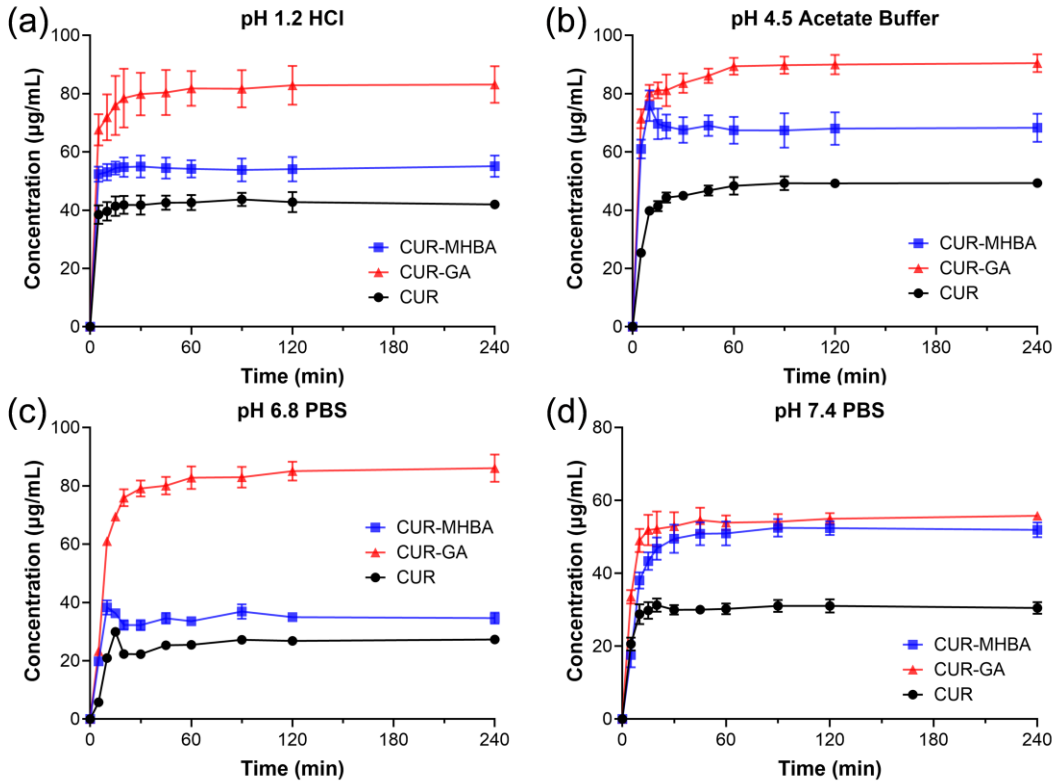

Figure 8. Powder dissolution profiles of CUR and its cocrystals in (a) pH 1.2,(b) pH 4.5,(c) pH 6.8 and (d) pH 7.4 buffer solution .

3.7. Antioxidant Activity Analysis

The antioxidant capacities of CUR and its cocrystals as well as their corresponding PM were evaluated using DPPH, ABTS, and FRAP assays (Figure 9). Lower IC_{50} values indicate stronger antioxidant activity.

In the DPPH assay, radical scavenging occurs through electron donation, reducing absorption at 517 nm proportionally to antioxidant strength.[66] Concentration-dependent scavenging was observed from 1.25 to 40 μg/mL. At 40 μg/mL, CUR-MHBA and CUR-GA exhibited scavenging rates of 64.95±2.17% and 73.03±2.77%, respectively, compared to 50.99±8.18% for CUR (Figure 9a), corresponding to 1.29-fold and 1.43-fold enhancements. The IC_{50} values were 31.70±3.18 μg/mL for CUR, 20.13±4.50 μg/mL for CUR-MHBA, and 13.27±4.26 μg/mL for CUR-GA. For comparison, the IC_{50} values of the physical mixtures were 31.89±3.80 μg/mL for CUR-MHBA PM and 25.77±3.05 μg/mL for CUR-GA PM. The cocrystals exhibited lower IC_{50} values than the corresponding physical mixtures, indicating improved apparent radical scavenging performance under the tested assay conditions.

In the ABTS assay, signal reduction at 734 nm reflects radical inhibition capacity.[67] At 32 μg/mL, both cocrystals outperformed CUR, with CUR-GA showing the strongest activity (IC_{50} = 6.06±1.91 μg/mL). CUR-MHBA and CUR-GA demonstrated 1.43-fold and 1.47-fold improvements, respectively, in radical scavenging compared to CUR (Figure 9b). The IC_{50} values of CUR-MHBA PM and CUR-GA PM were 30.21±1.46 μg/mL and 18.18±2.47 μg/mL, respectively. The IC_{50} values of the cocrystals were lower than those of the corresponding PM.

The FRAP assay measures reduction of Fe^{3+}-TPTZ to Fe^{2+}-TPTZ at 593 nm, where higher absorbance indicates greater reducing power.[68] CUR-MHBA and CUR-GA showed significantly greater activity above 5 μg/mL. At 40 μg/mL, reducing capacity was 3.48-fold higher for CUR-MHBA and 3.89-fold higher for CUR-GA than for CUR (Figure 9c).

The PM exhibited lower reducing capacity than the corresponding cocrystals across the tested concentration range, consistent with the radical scavenging assays. Overall, the cocrystals exhibited improved apparent antioxidant activity under the tested experimental conditions compared to CUR and their corresponding PM, which may be associated with differences in dissolution and dispersion behavior during the assay[69-71].

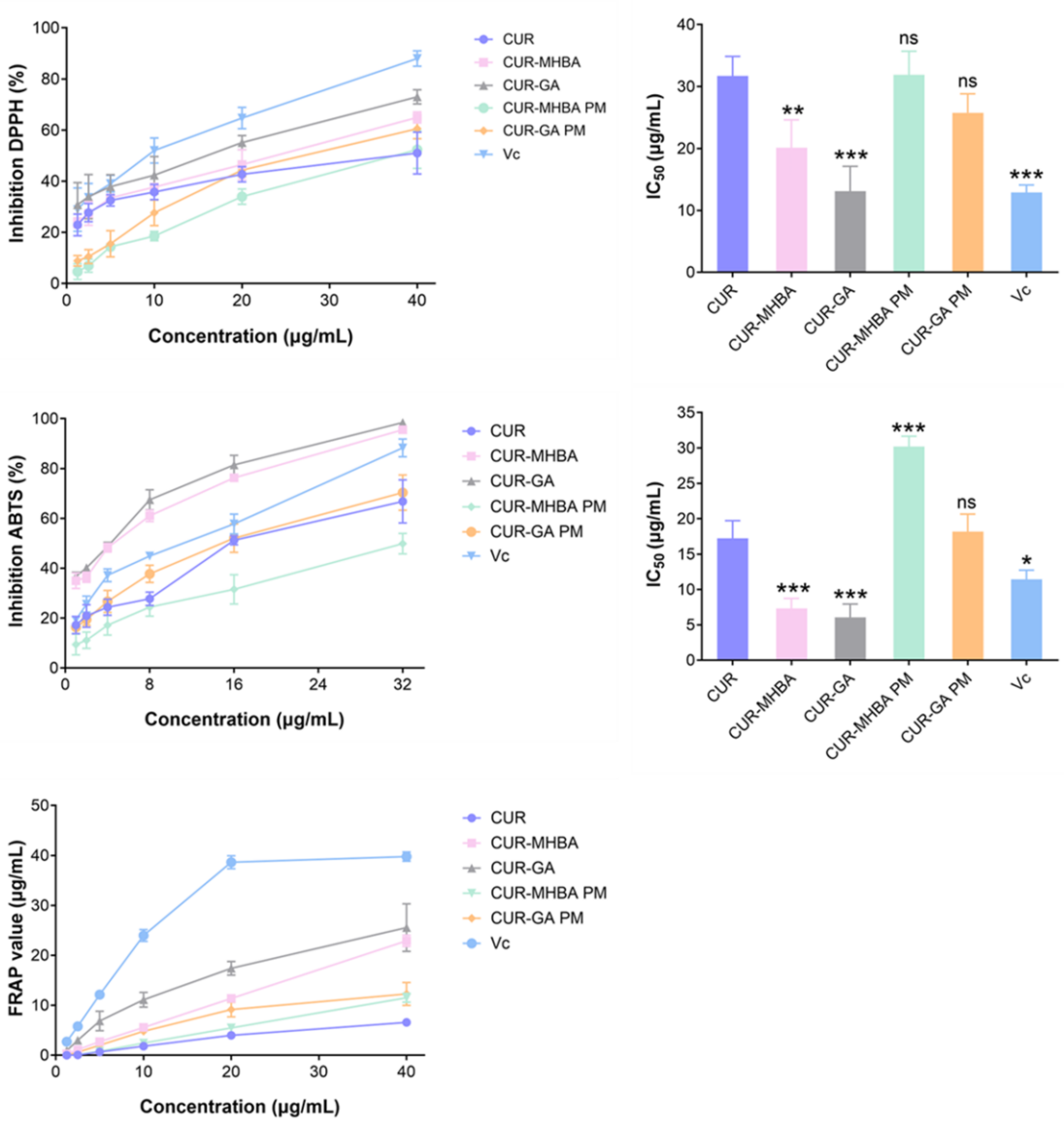

Figure 9. Antioxidant activity of CUR, cocrystals and corresponding PM by (a) DPPH,(b) ABTS, and (c) FRAP.

3.8. Antimicrobial Activity Analysis.

3.8.1. MIC Analysis

The antibacterial activities of CUR and its cocrystals against *S.aureus* and *E.coli* were determined using microbroth dilution with TTC staining validation (Figure 10). MIC values, defined as the lowest concentration preventing visible bacterial growth, served as the primary activity metric with triplicate parallel testing under all conditions.Red-outlined wells indicated the first concentration achieving complete growth inhibition. All cocrystals demonstrated significantly lower MIC values than

CUR against both strains: MIC against *S.aureus* decreased from 0.5 mg/mL for CUR to 0.25 mg/mL for cocrystals, while MIC against *E.coli* reduced from 1 mg/mL to 0.5 mg/mL. In contrast, CUR-MHBA PM and CUR-GA PM exhibited weaker antibacterial activity, with MIC values of 1 mg/mL against *S. aureus* and greater than 1 mg/mL against *E. coli*. These results suggest that the cocrystals exhibited improved apparent antibacterial activity under the tested experimental conditions compared with CUR and the corresponding physical mixtures. However, this observation should not be interpreted as evidence that cocrystallization alters the intrinsic antibacterial activity of dissolved CUR, and may instead be related to differences in dissolution and dispersion behavior during the assay[48,72].

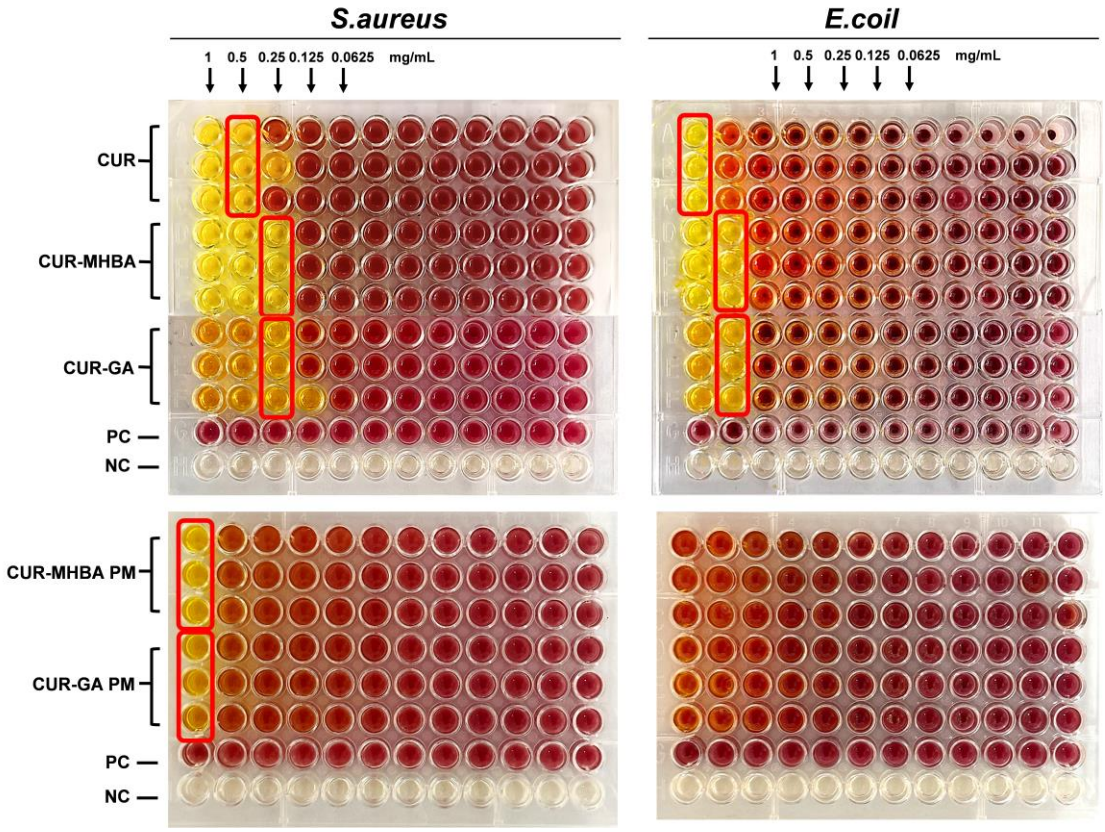

Figure 10. Images of CUR, cocrystals and corresponding PM tested for antibacterial activity against *S.aureus* and *E.coli* in vitro using the 96-well plate method. The red rectangle represents the location of the minimum inhibitory concentration of solution clarity.

3.8.2. Growth Curve Kinetics Analysis

To dynamically evaluate the antibacterial efficacy of CUR and its cocrystals, growth curves of *S.aureus* and *E.coli* were monitored by measuring OD_{600} at designated

time points post-treatment (Figure 10).

For *S.aureus* shown in Figure 10(a-c), both cocrystal-treated groups exhibited growth curves below those of CUR across all concentrations, indicating stronger inhibitory effects. At a sub-MIC concentration of 0.125 mg/mL, CUR allowed rapid exponential growth within 0–24 h, followed by a stationary phase. In contrast, cocrystals at the same concentration significantly delayed entry into the logarithmic phase and maintained lower OD_{600} values throughout, demonstrating effective suppression of bacterial growth even at subinhibitory levels. CUR-MHBA and CUR-GA showed particularly strong inhibition: although bacteria entered the logarithmic phase between 6–24 h, they exhibited lower growth rates and reduced growth amplitude, reaching stationary phase by 24 h.

Against *E.coli* depicted in Figure 10(d-f), although the cocrystals showed lower MIC values indicating enhanced antibacterial activity, differences in growth curves were less pronounced than those against *S.aureus*. This is consistent with literature reports that CUR has stronger membrane-disrupting effects on Gram-positive bacteria such as *S.aureus* than on Gram-negative bacteria like *E.coli* [68]. Altogether, these findings suggest that cocrystallization enhances antibacterial activity of CUR, likely through improved solubility.

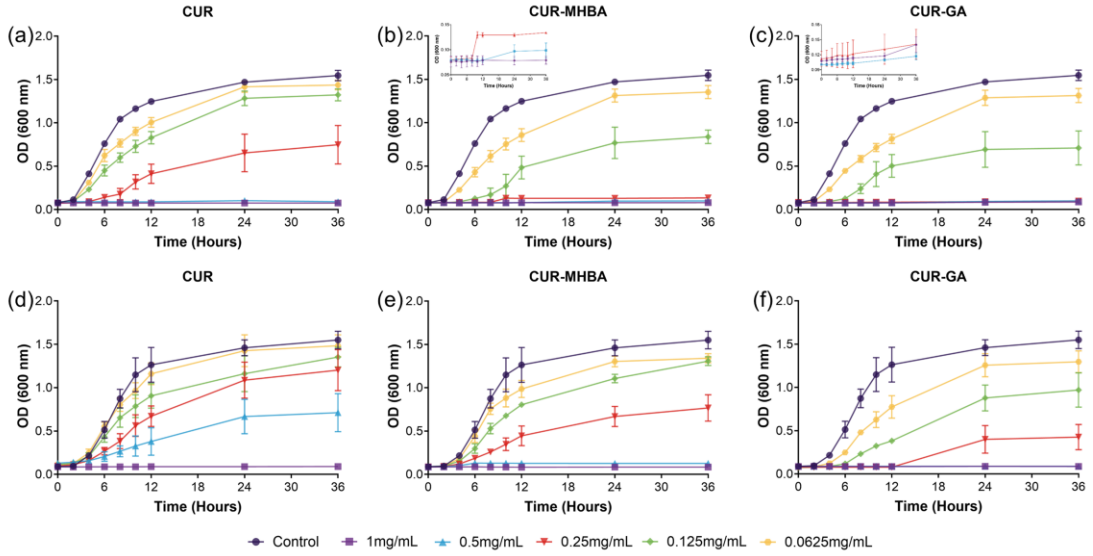

Figure 11. Growth curve kinetics displaying the effect of CUR and its cocrystals on the growth of (a-c) *S.aureus* and (d-f) *E.coli. S.aureus* and *E.coli* WT cells without any drug treatment were taken as respective controls.

3.8.3. Zone of Inhibition Analysis

To comprehensively evaluate the antibacterial activity of the CUR cocrystals, the agar well diffusion assay was used to assess the inhibitory effects of CUR, CUR-MHBA, and CUR-GA against *S.aureus* and *E.coli*. Based on MIC results, concentrations of 0.5, 1, and 2 mg/mL were selected for S. aureus (CUR MIC = 0.5 mg/mL), and 1, 2, and 3 mg/mL for E. coli (CUR MIC = 1 mg/mL). This design allowed evaluation of diffusion capacity and antibacterial efficacy at subinhibitory, inhibitory, and supratherapeutic concentrations.

As shown in Figure 11, both cocrystals produced significantly larger inhibition zones than CUR at equivalent concentrations against both pathogens. These results are consistent with the reduced MIC values observed in broth dilution assays and enhanced growth suppression in kinetic analyses, confirming the superior antibacterial activity of the cocrystals over CUR alone.

Against *S.aureus* (Figure 11(a-b)), the inhibitory efficacy ranked CUR-MHBA ≈ CUR-GA > CUR, aligning with the strong growth inhibition observed in kinetic studies. For *E.coli* (Figure 11(c-d)), a similar trend was observed: CUR-GA > CUR-MHBA > CUR. The slightly enhanced performance of CUR-GA may be attributed to its electron-donating capacity, as indicated in antioxidant assays. No inhibition zones were observed for DMSO or the individual coformers, confirming the absence of solvent or single-component interference and suggesting synergistic antibacterial effects in the cocrystals.

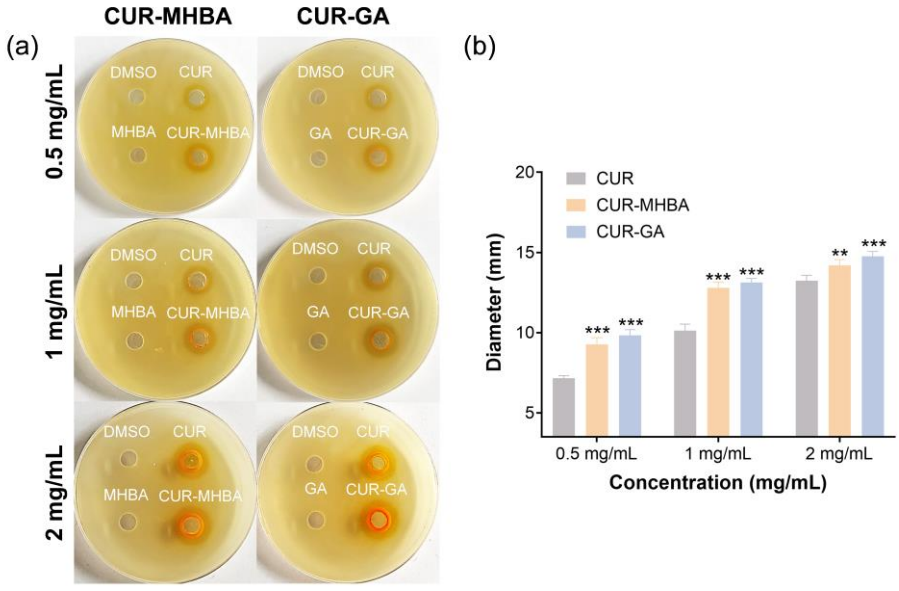

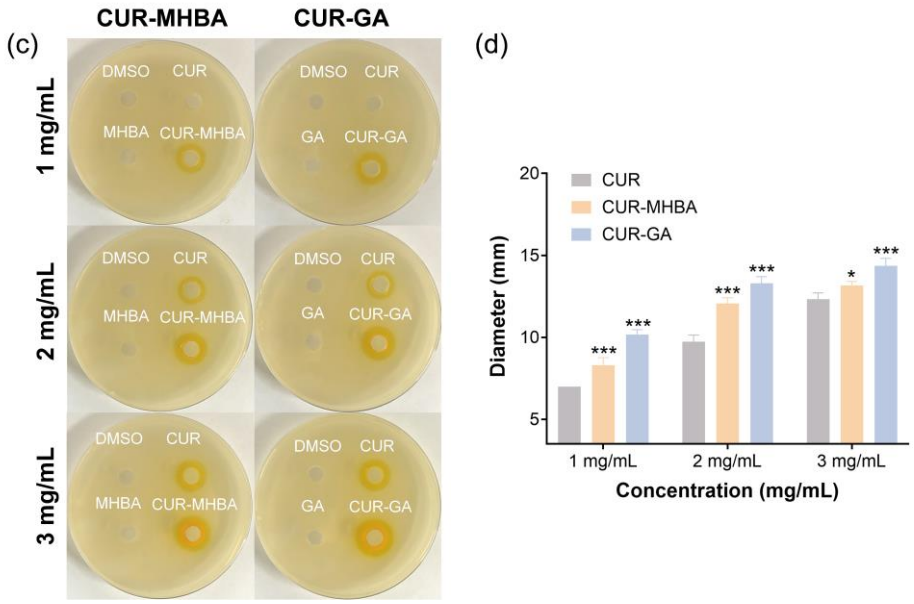

Figure 12. Agar diffusion assay of CUR and its cocrystals: Representative inhibition zones against (a-b)*S. aureus* and (c-d) *E.coli* and Comparative diameter analysis of zones.

3.9. Stability Study

The PXRD patterns of both cocrystals recorded at 0, 7, and 14 days exhibited identical diffraction peak positions without the appearance of any new peaks or disappearance of characteristic reflections (Figure 12). Although minor variations in peak intensities were observed, these changes are commonly attributed to differences in sample packing density and preferred orientation effects during PXRD measurement rather than to a structural transformation. These results indicate that no phase transition or dissociation occurred under the storage conditions (25°C and 75% RH), suggesting that the cocrystals remained structurally stable in the solid state during the investigated period. However, the present experiment was designed to evaluate solid-state stability, and the solution-state behavior of the cocrystals was not investigated in this study.

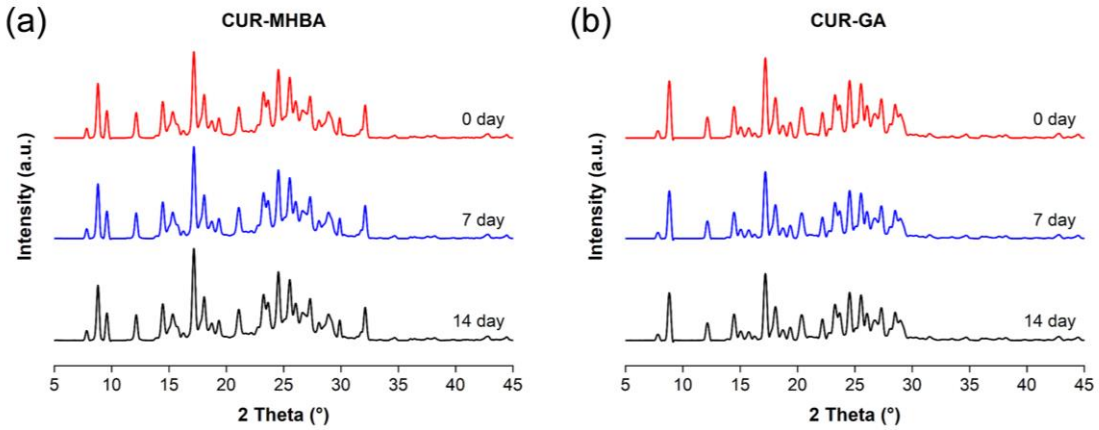

Figure 13. PXRD patterns of CUR-MHBA and CUR-GA cocrystals during stability testing at 25°C and 75% RH (0, 7, and 14 days).

4. CONCLUSION

This study successfully engineered two novel cocrystals through co-crystallization of CUR with bioactive polyphenolic coformers. Comprehensive characterization via PXRD, DSC, TG, IR, and ^{1}H-NMR confirmed their structural integrity and thermal stability. Equilibrium solubility and powder dissolution studies demonstrated substantial enhancements in solubility, dissolution rate, and peak concentration. Crucially, these superior dissolution properties translated to enhanced bioactivity. DPPH, ABTS, and FRAP assays revealed synergistic antioxidant enhancement between CUR and coformers. Concurrently, both of cocrystals exhibited significantly reduced MIC values. These findings collectively establish that selecting coformers with dual functionality, crystal engineering capability and intrinsic bioactivity, provides an effective strategy for simultaneously improving the dissolution performance of CUR and amplifying its antioxidant/antibacterial efficacy. The CUR cocrystal breakthrough not only facilitates development of high-efficiency CUR formulations but also offers a valuable paradigm for optimizing other natural polyphenolic or diketone-based active compounds with analogous structural features.

References

1. Sanphui P, Bolla G. Curcumin, a biological wonder molecule: A crystal engineering point of view. *Crystal Growth & Design* 2018;18(9):5690-711. doi: 10.1021/acs.cgd.8b00646
2. Suresh K, Nangia A. Curcumin: Pharmaceutical solids as a platform to improve solubility and bioavailability. *CrystEngComm* 2018;20(24):3277-96. doi: 10.1039/c8ce00469b
3. DerMarderosian A, Beutler JA. The review of natural products: The most complete

source of natural product information 2002. doi: 10.5555/20033079649
4. Tyagi P, Singh M, Kumari H, Kumari A, Mukhopadhyay K. Bactericidal activity of curcumin i is associated with damaging of bacterial membrane. *PloS One* 2015;10(3):e0121313. doi: 10.1371/journal.pone.0121313
5. Chainani-Wu N. Safety and anti-inflammatory activity of curcumin: A component of tumeric (curcuma longa). *The Journal of Alternative & Complementary Medicine* 2003;9(1):161-8. doi: 10.1089/107555303321223035
6. Liu S, Wang Z, Hu Z, Zeng X, Li Y, Su Y, et al. Anti-tumor activity of curcumin against androgen-independent prostate cancer cells via inhibition of nf-κb and ap-1 pathway in vitro. *Journal of Huazhong University of Science and Technology [Medical Sciences]* 2011;31(4):530-4. doi: 10.1007/s11596-011-0485-1
7. Wilken R, Veena MS, Wang MB, Srivatsan ES. Curcumin: A review of anti-cancer properties and therapeutic activity in head and neck squamous cell carcinoma. *Molecular Cancer* 2011;10(1):12. doi: 10.1186/1476-4598-10-12
8. Chen S, Wu J, Tang Q, Xu C, Huang Y, Huang D, et al. Nano-micelles based on hydroxyethyl starch-curcumin conjugates for improved stability, antioxidant and anticancer activity of curcumin. *Carbohydrate Polymers* 2020;228:115398. doi: 10.1016/j.carbpol.2019.115398
9. Farzaei MH, Zobeiri M, Parvizi F, El-Senduny FF, Marmouzi I, Coy-Barrera E, et al. Curcumin in liver diseases: A systematic review of the cellular mechanisms of oxidative stress and clinical perspective. *Nutrients* 2018;10(7):855. doi: 10.3390/nu10070855
10. Patel SS, Acharya A, Ray R, Agrawal R, Raghuwanshi R, Jain P. Cellular and molecular mechanisms of curcumin in prevention and treatment of disease. *Critical reviews in food science and nutrition* 2020;60(6):887-939. doi: 10.1080/10408398.2018.1552244
11. Baum L, Lam CWK, Cheung SK-K, Kwok T, Lui V, Tsoh J, et al. Six-month randomized, placebo-controlled, double-blind, pilot clinical trial of curcumin in patients with alzheimer disease. *Journal of clinical psychopharmacology* 2008;28(1):110-3. doi: 10.1097/jcp.0b013e318160862c
12. Olotu F, Agoni C, Soremekun O, Soliman ME. An update on the pharmacological usage of curcumin: Has it failed in the drug discovery pipeline? *Cell Biochemistry and Biophysics* 2020;78(3):267-89. doi: 10.1007/s12013-020-00922-5
13. Basford PA, Cameron CA, Cruz-Cabeza AJ. Conformational change initiates dehydration in fluconazole monohydrate. *Crystal Growth & Design* 2020;20(9):6044-56. doi: 10.1021/acs.cgd.0c00768
14. Alkhamis KA, Obaidat AA, Nuseirat AF. Solid-state characterization of fluconazole. *Pharmaceutical development and technology* 2002;7(4):491-503. doi: 10.1081/PDT-120015052
15. Charoo N, Cristofoletti R, Graham A, Lartey P, Abrahamsson B, Groot D, et al. Biowaiver monograph for immediate-release solid oral dosage forms: Fluconazole. *Journal of Pharmaceutical Sciences* 2014;103(12):3843-58. doi: 10.1002/jps.24181
16. Kavanagh ON, Croker DM, Walker GM, Zaworotko MJ. Pharmaceutical cocrystals: From serendipity to design to application. *Drug Discovery Today* 2019;24(3):796-804.

doi: 10.1016/j.drudis.2018.11.023
17. Bolla G, Nangia A. Pharmaceutical cocrystals: Walking the talk. *Chemical communications* 2016;52(54):8342-60. doi: 10.1039/C6CC02943D
18. Qiao N, Li M, Schlindwein W, Malek N, Davies A, Trappitt G. Pharmaceutical cocrystals: An overview. *International Journal of Pharmaceutics* 2011;419(1-2):1-11. doi: 10.1016/j.ijpharm.2011.07.037
19. Remenar JF, Morissette SL, Peterson ML, Moulton B, MacPhee JM, Guzmán HR, et al. Crystal engineering of novel cocrystals of a triazole drug with 1, 4-dicarboxylic acids. *Journal of the American Chemical Society* 2003;125(28):8456-7. doi: 10.1021/ja035776p
20. Cheney ML, Weyna DR, Shan N, Hanna M, Wojtas L, Zaworotko MJ. Coformer selection in pharmaceutical cocrystal development: A case study of a meloxicam aspirin cocrystal that exhibits enhanced solubility and pharmacokinetics. *Journal of Pharmaceutical Sciences* 2011;100(6):2172-81. doi: 10.1002/jps.22434
21. McNamara DP, Childs SL, Giordano J, Iarriccio A, Cassidy J, Shet MS, et al. Use of a glutaric acid cocrystal to improve oral bioavailability of a low solubility api. *Pharmaceutical Research* 2006;23(8):1888-97. doi: 10.1007/s11095-006-9032-3
22. Bak A, Gore A, Yanez E, Stanton M, Tufekcic S, Syed R, et al. The co-crystal approach to improve the exposure of a water-insoluble compound: Amg 517 sorbic acid co-crystal characterization and pharmacokinetics. *Journal of Pharmaceutical Sciences* 2008;97(9):3942-56. doi: 10.1002/jps.21280
23. Karki S, Friščić T, Jones W. Control and interconversion of cocrystal stoichiometry in grinding: Stepwise mechanism for the formation of a hydrogen-bonded cocrystal. *CrystEngComm* 2009;11(3):470-81. doi: 10.1039/B812531G
24. Zhang H, Guo C, Wang X, Xu J, He X, Liu Y, et al. Five energetic cocrystals of btf by intermolecular hydrogen bond and π-stacking interactions. *Crystal Growth & Design* 2013;13(2):679-87. doi: 10.1021/cg301353f
25. Saha S, Desiraju GR. Acid⋯ amide supramolecular synthon in cocrystals: From spectroscopic detection to property engineering. *Journal of the American Chemical Society* 2018;140(20):6361-73. doi: 10.1021/jacs.8b02435
26. Adalder TK, Sankolli R, Dastidar P. Homo-or heterosynthon? A crystallographic study on a series of new cocrystals derived from pyrazinecarboxamide and various carboxylic acids equipped with additional hydrogen bonding sites. *Crystal Growth & Design* 2012;12(5):2533-42. doi: 10.1021/cg300140w
27. Babu NJ, Reddy LS, Nangia A. Amide− n-oxide heterosynthon and amide dimer homosynthon in cocrystals of carboxamide drugs and pyridine n-oxides. *Molecular Pharmaceutics* 2007;4(3):417-34. doi: 10.1021/mp070014c
28. Tothadi S, Desiraju GR. Synthon modularity in 4-hydroxybenzamide–dicarboxylic acid cocrystals. *Crystal Growth & Design* 2012;12(12):6188-98. doi: 10.1021/cg3013766
29. Sudhakar P, Srivijaya R, Sreekanth B, Jayanthi P, Vishweshwar P, Babu MJ, et al. Carboxylic acid–pyridine supramolecular heterocatemer in a co-crystal. *Journal of Molecular Structure* 2008;885(1-3):45-9. doi: 10.1016/j.molstruc.2007.10.003

30. Sarmah KK, Rajbongshi T, Bhowmick S, Thakuria R. First-line antituberculosis drug, pyrazinamide, its pharmaceutically relevant cocrystals and a salt. *Structural Science* 2017;73(5):1007-16. doi: 10.1107/S2052520617011477
31. Albadri AA, Jihad MI, Radhi ZA. Preparation, characterization, and in-vitro evaluation of tenoxicam-paracetamol cocrystal. *International Journal of Drug Deliver y Technology* 2021;10:542-6. doi: 10.25258/ijddt.10.4.6
32. Qiao S, Wang J, Yu Y, Liu Y, Yang Z, Li H. Two novel tnb energetic cocrystals with low melting point: A potential strategy to construct melt cast explosive carriers. *CrystEngComm* 2022;24(16):2948-53. doi: 10.1039/D2CE00025C
33. Gong N, Zhang Y, Wang Y, Yu H, Zhang B, Zhang H, et al. Versatile salts as a strategy to modify the biopharmaceutical properties of venlafaxine and a potential hypoglycemic effect study. *Crystal Growth & Design* 2020;20(5):3131-9. doi: 10.1021/acs.cgd.0c00007
34. Wang J, Dai X-L, Lu T-B, Chen J-M. Temozolomide–hesperetin drug–drug cocrystal with optimized performance in stability, dissolution, and tabletability. *Crystal Growth & Design* 2021;21(2):838-46. doi: 10.1021/acs.cgd.0c01153
35. Almansa C, Merce R, Tesson N, Farran J, Tomas J, Plata-Salamán CR. Co-crystal of tramadol hydrochloride–celecoxib (ctc): A novel api–api co-crystal for the treatment of pain. *Crystal Growth & Design* 2017;17(4):1884-92. doi: 10.1021/acs.cgd.6b01848
36. Shinozaki T, Ono M, Higashi K, Moribe K. A novel drug-drug cocrystal of levofloxacin and metacetamol: Reduced hygroscopicity and improved photostability of levofloxacin. *Journal of Pharmaceutical Sciences* 2019;108(7):2383-90. doi: 10.1016/j.xphs.2019.02.014
37. Wang L-Y, Bu F-Z, Li Y-T, Wu Z-Y, Yan C-W. A sulfathiazole–amantadine hydrochloride cocrystal: The first codrug simultaneously comprising antiviral and antibacterial components. *Crystal Growth & Design* 2020;20(5):3236-46. doi: 10.1021/acs.cgd.0c00075
38. Sanphui P, Goud NR, Khandavilli UBR, Nangia A. Fast dissolving curcumin cocrystals. *Crystal Growth & Design* 2011;11(9):4135-45. doi: 10.1021/cg200704s
39. Kho K, Nugroho D, Sugih AK. Preparation and characterization of highly water soluble curcumin–dextrose cocrystal. *The Journal of Pure and Applied Chemistry Research* 2018;7(2):140. doi: 123456789/7097
40. Su H, He H, Tian Y, Zhao N, Sun F, Zhang X, et al. Syntheses and characterizations of two curcumin-based cocrystals. *Inorganic Chemistry Communications* 2015;55:92-5. doi: 10.1016/j.inoche.2015.03.027
41. Rathi N, Paradkar A, Gaikar VG. Polymorphs of curcumin and its cocrystals with cinnamic acid. *Journal of Pharmaceutical Sciences* 2019;108(8):2505-16. doi: 10.1016/j.xphs.2019.03.014
42. Sathisaran I, Dalvi SV. Crystal engineering of curcumin with salicylic acid and hydroxyquinol as coformers. *Crystal Growth & Design* 2017;17(7):3974-88. doi: 10.1021/acs.cgd.7b00599
43. Shen R, Zhang J, Wang X. Cocrystal of curcumin with 4,4 ' -bipyridine toward improved dissolution: Design, structure analysis, and solid-state characterization.

Journal of Molecular Structure 2023;1284. doi: 10.1016/j.molstruc.2023.135348
44. Wang H, Zheng C, Tian F, Xiao Z, Sun Z, Lu L, et al. Improving the dissolution rate and bioavailability of curcumin via co-crystallization. *Pharmaceuticals* 2024;17(4):489. doi: 10.3390/ph17040489
45. Chow SF, Shi L, Ng WW, Leung KHY, Nagapudi K, Sun CC, et al. Kinetic entrapment of a hidden curcumin cocrystal with phloroglucinol. *Crystal Growth & Design* 2014;14(10):5079-89. doi: 10.1021/cg5007007
46. Xuan B, Chen YCS, Wong KC, Chen R, Lo PS, Lakerveld R, et al. Impact of cocrystal solution-state stability on cocrystal dissociation and polymorphic drug recrystallization during dissolution. *International Journal of Pharmaceutics* 2021;610:121239. doi: 10.1016/j.ijpharm.2021.121239
47. Glomme A, März J, Dressman JB. Comparison of a miniaturized shake-flask solubility method with automated potentiometric acid/base titrations and calculated solubilities. *Journal of Pharmaceutical Sciences* 2005;94(1):1-16. doi: 10.1002/jps.20212
48. Schultheiss N, Newman A. Pharmaceutical cocrystals and their physicochemical properties. *Crystal Growth & Design* 2009;9(6):2950-67. doi: 10.1021/cg900129f
49. Zhou Y, Tu Y, Yang J, Qian K, Liu X, Fu Q, et al. Enhancing the stability, solubility, and antioxidant activity of cinchonine through pharmaceutical cocrystallization. *Pharmaceutical Research* 2024;41(6):1257-70. doi:10.1007/s11095-024-03712-3
50. Mitic V, Jovanovic VS, Dimitrijevic M, Cvetkovic J, Simonovic S, Mandic SN. Chemometric analysis of antioxidant activity and anthocyanin content of selected wild and cultivated small fruit from serbia. *Fruits* 2014;69(5):413-22. doi: 10.1051/fruits/2014026
51. Rozi P, Abuduwaili A, Mutailifu P, Gao Y, Rakhmanberdieva R, Aisa HA, et al. Sequential extraction, characterization and antioxidant activity of polysaccharides from fritillaria pallidiflora schrenk. *International Journal of Biological Macromolecules* 2019;131:97-106. doi: 10.1016/j.ijbiomac.2019.03.029
52. Benzie IF, Strain JJ. The ferric reducing ability of plasma (frap) as a measure of "antioxidant power": The frap assay. *Analytical Biochemistry* 1996;239(1):70-6. doi: 10.1006/abio.1996.0292
53. Veiga A, Maria da Graça TT, Rossa LS, Mengarda M, Stofella NC, Oliveira LJ, et al. Colorimetric microdilution assay: Validation of a standard method for determination of mic, ic50%, and ic90% of antimicrobial compounds. *Journal of Microbiological Methods* 2019;162:50-61. doi: 10.1016/j.mimet.2019.05.003
54. Saifullah B, Buskaran K, Shaikh RB, Barahuie F, Fakurazi S, Mohd Moklas MA, et al. Graphene oxide–peg–protocatechuic acid nanocomposite formulation with improved anticancer properties. *Nanomaterials* 2018;8(10):820. doi: 10.3390/nano8100820
55. Serrano DR, Persoons T, D'Arcy DM, Galiana C, Dea-Ayuela MA, Healy AM. Modelling and shadowgraph imaging of cocrystal dissolution and assessment of in vitro antimicrobial activity for sulfadimidine/4-aminosalicylic acid cocrystals. *European Journal of Pharmaceutical Sciences* 2016;89:125-36. doi: 10.3390/cryst13040640

56. Chernyshev VV. Structural characterization of pharmaceutical cocrystals with the use of laboratory x-ray powder diffraction patterns. *Crystals* 2023;13(4). doi: 10.3390/cryst13040640
57. Saganowska P, Wesolowski M. Dsc as a screening tool for rapid co-crystal detection in binary mixtures of benzodiazepines with co-formers. *Journal of Thermal Analysis and Calorimetry* 2018;133(1):785-95. doi: 10.1007/s10973-017-6858-3
58. Lu E, Rodríguez-Hornedo N, Suryanarayanan R. A rapid thermal method for cocrystal screening. *CrystEngComm* 2008;10(6):665-8. doi: 10.1039/B801713C
59. Vemuri VD, Lankalapalli S. Rosuvastatin cocrystals: An attempt to modulate physicochemical parameters. *Future Journal of Pharmaceutical Sciences* 2021;7(1):64. doi: 10.1186/s43094-021-00213-7
60. Meng Y, Tan F, Yao J, Cui Y, Feng Y, Li Z, et al. Preparation, characterization, and pharmacokinetics of rivaroxaban cocrystals with enhanced in vitro and in vivo properties in beagle dogs. *International Journal of Pharmaceutics-X* 2022;4. doi: 10.1016/j.ijpx.2022.100119
61. Guo X, Guo Y, Zhang M, Yang B, Liu H, Yin T, et al. A comparative study on in vitro and in vivo characteristics of enzalutamide nanocrystals versus amorphous solid dispersions and a better prediction for bioavailability based on “spring-parachute” model. *International Journal of Pharmaceutics* 2022;628:122333. doi: 10.1016/j.ijpharm.2022.122333
62. Hu C, Liu Z, Liu C, Li J, Wang Z, Xu L, et al. Enhanced oral bioavailability and anti-echinococcosis efficacy of albendazole achieved by optimizing the “spring” and “parachute”. *Molecular Pharmaceutics* 2019;16(12):4978-86. doi: 10.1021/acs.molpharmaceut.9b00851
63. Du R, Xu J, Zhang L, Ning L, Li S. Ethinyl estradiol cocrystals assembled by chain structures: Improvement in stability and solubility. *New Journal of Chemistry* 2019;43(43):16889-97. doi: 10.1039/c9nj04147h
64. Wei Y, Zhang L, Wang N, Shen P, Dou H, Ma K, et al. Mechanistic study on complexation-induced spring and hover dissolution behavior of ibuprofen-nicotinamide cocrystal. *Crystal Growth & Design* 2018;18(12):7343-55. doi: 10.1021/acs.cgd.8b00978
65. Rathod V, Stagner WC, Gajera B, Haware RV. Hybridized nanoamorphous micellar dispersion using a qbd–dm3 linked rational product design strategy for ritonavir: A bcs iv drug. *International Journal of Pharmaceutics* 2020;588:119727. doi: 10.1016/j.ijpharm.2020.119727
66. Baranowska I, Bajkacz S. A new uhplc-ms/ms method for the determination of flavonoids in supplements and dpph[•]-uhplc-uv method for the evaluation of the radical scavenging activity of flavonoids. *Food Chemistry* 2018;256:333-41. doi: 10.1016/j.foodchem.2018.02.138
67. Ilyasov IR, Beloborodov VL, Selivanova IA, Terekhov RP. Abts/pp decolorization assay of antioxidant capacity reaction pathways. *International Journal of Molecular Sciences* 2020;21(3). doi: 10.3390/ijms21031131
68. Benzie IFF, Choi S-W. Antioxidants in food: Content, measurement, significance,

action, cautions, caveats, and research needs. *Advances in food and nutrition research* 2014;71:1-53. doi: 10.1016/b978-0-12-800270-4.00001-8
69. Shan N, Zaworotko MJ. The role of cocrystals in pharmaceutical science. *Drug Discovery Today* 2008;13(9-10):440-6. doi: 10.1016/j.drudis.2008.03.004
70. Jayram P, Sudheer P. Pharmaceutical co-crystals: A systematic review. *International Journal of Pharmaceutical Investigation* 2020;10(3). doi: 10.5330/ijpi.2020.3.45
71. Anand P, Kunnumakkara AB, Newman RA, Aggarwal BB. Bioavailability of curcumin: Problems and promises. *Molecular Pharmaceutics* 2007;4(6):807-18. doi: 10.1021/mp700113r
72. Savjani KT, Gajjar AK, Savjani JK. Drug solubility: Importance and enhancement techniques. *International Scholarly Research Notices* 2012;2012(1):195727. doi: 10.5402/2012/195727